AIAA JOURNAL
Vol. 36, No. 9, September 1998

Nozzle Flow Separation

G. L. Romine*
Lockheed Martin Astronautics, Denver, Colorado 80201

During the sea-level ignition process of rocket motors, the nozzle is subjected to an overexpanded flow condition that can cause high side loads. Prediction of the symmetrical separation location is the first key step to a determination of the range of possible side-load magnitudes. The mechanisms responsible for causing the flow to separate from the nozzle wall are demonstrated, and the theory for a new solution of the separation location is presented. The model is also correlated with historical rocket data, a new approximate solution, and an empirical curve fit that has been in use for 35 years.

Nomenclature

A	= cross-sectional area of nozzle
B	= constant in approximate solution
C	= constant in Schilling curve fit
C_D	= discharge coefficient
E	= exponent in Schilling curve fit
F	= thrust
M	= Mach number
$\dot{m}$	= mass flow rate
p	= pressure
V	= velocity
α	= ratio of Mach disk area to nozzle area at separation point A_{Md}/A_3
γ	= ratio of specific heats
δ	= flow deflection across shock
θ	= flow angle
θ_N	= nozzle half-angle
ξ_{12}	= pressure ratio across shock, p_2/p_1
ρ	= density
ϕ	= shock angle

Subscripts

amb	= ambient
c	= chamber
Md	= Mach disk
sep	= separation point
wall	= nozzle wall
1	= upstream of shock, strong and weak solutions
2	= downstream of shock, strong and weak solutions
3	= upstream of oblique shock at separation point
4	= downstream of oblique shock at separation point
4tp	= downstream of incident shock at triple point
5	= upstream of triple point
6strong	= downstream of Mach disk
6weak	= downstream of reflected shock at triple point

Superscripts

$\bar{V}$	= average velocity across jet
$\bar{\rho}$	= average density across jet
$*$	= conditions at nozzle throat

Introduction

THE first flight of the Titan IVB launch vehicle with its new solid rocket motor upgrade (SRMU) gave unexpectedly high nozzle actuator loads during ignition. The ensuing effort to define the root cause converged on asymmetrical flow separation in the nozzles. To understand root cause before the next Titan IVB flight using the SRMU (the Cassini mission to Saturn), all aspects of the problem came under scrutiny, including development of a reliable method to predict symmetrical flow separation. Work in the early 1960s and 1970s produced a number of theories and a large volume of separation data; however, the underlying physical mechanism behind separation was not totally clear, and correlation with data was difficult at best. Morrisette and Goldberg[1] provide a good summary of the situation. For preliminary SRMU calculations, the model of Arens and Spiegler[2] was used. To provide an independent calculation, the work of Schilling[3] was subsequently utilized because it is an empirical curve fit to the data and is far easier to use in sensitivity studies. Both techniques were close in predicting flow separation but suffer from a lack of a basic physical justification. In an effort to add to the understanding of the phenomena, this study focuses on the overall separation process and yields a direct solution, an approximate solution, and confirmation of the efficiency of the Schilling curve fit that was used in the SRMU analyses.

Jet Flow Structure

The boundary condition encountered by an expanding nozzle flow is a constant ambient pressure. The process of pressure adjustment produces a complicated shock structure in the separated jet that alternates from overexpansion to overcompression, which is shown by the repeating shock diamonds or cells (Fig. 1). The first one or two cells usually contain a Mach disk across the axis terminating at a triple point. The initial triple point has an incident shock that originates at the separation point on the nozzle wall, a reflected shock, a normal shock or Mach disk, and a slipstream separating supersonic and subsonic flows aft of the triple point. Of primary importance is the first complete cell after the flow has separated. Subsequent cells are disrupted by shear layers at the boundary and slipstream and by vorticity gradients from the shocks; thus, their shock structure is not as sharply defined. The adverse pressure gradient necessary to separate the mainstream flow and the nozzle boundary layer from the wall is supplied by the separation shock. The shock originates at the separation point, but its strength and location are dictated by the overall adjustment process of the complete first cell, where all parts are controlled by the ambient pressure boundary condition. The proposed flow separation model is dictated by the jet mainstream adjustment to ambient pressure and not by the condition of the nozzle boundary layer.

Flow Separation Model

Nozzle flow separation may occur when the ambient pressure lies between two limits, the nozzle static pressure at the lip resulting from subsonic compression after reaching sonic velocity at the throat and the nozzle static pressure at the lip from supersonic expansion. Between these two limits, nozzle flow separation is driven by the manner in which the flow adjusts to the ambient pressure. The proposed model is bounded by two ideal cases: 1) the ideal nozzle flow case or classical solution and 2) the ideal jet flow case. It will be

Received Nov. 28, 1997; revision received May 11, 1998; accepted for publication May 18, 1998. Copyright © 1998 by the American Institute of Aeronautics and Astronautics, Inc. All rights reserved.

*Department Staff Engineer, Titan Technical Integration, P.O. Box 179. Senior Member AIAA.

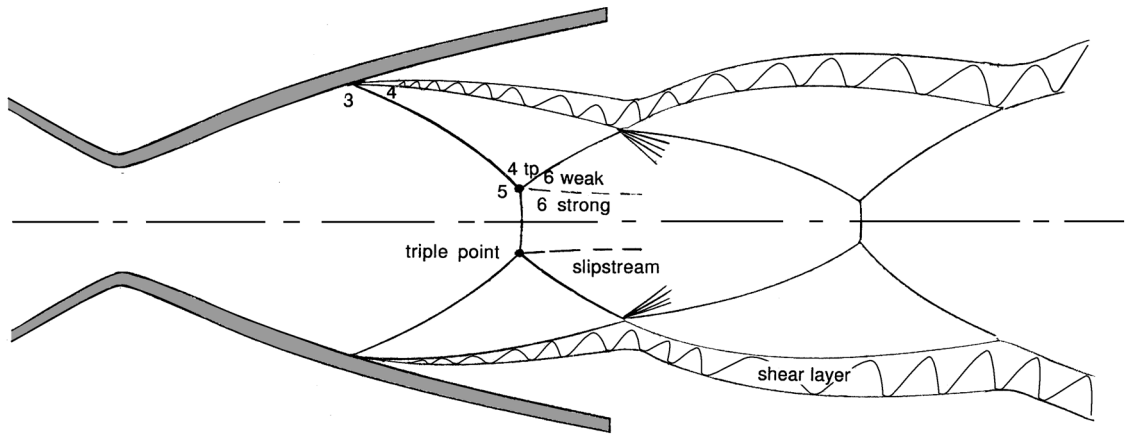

Fig. 1 Jet flow structure.

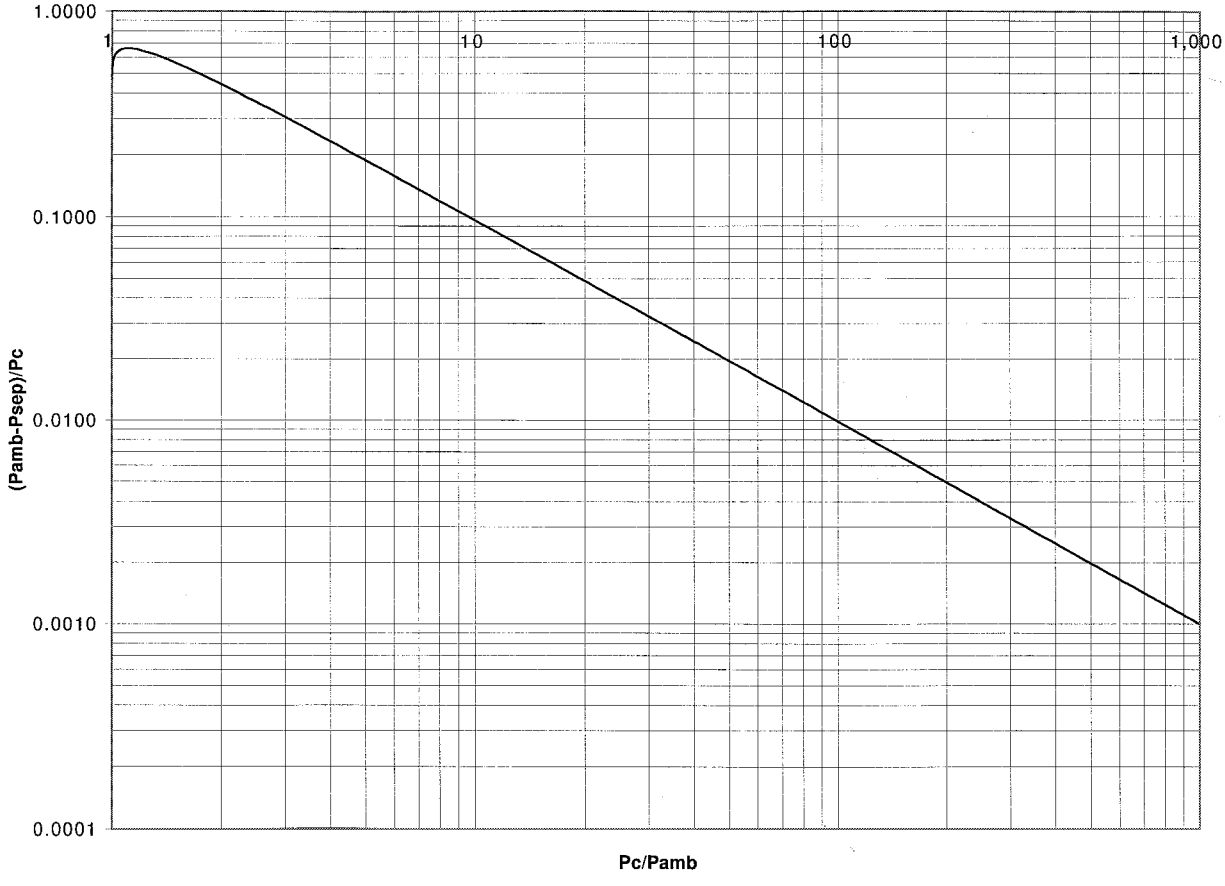

Fig. 2 Separation pressure from ideal nozzle flow case.

shown that only the proposed triple-point solution is valid based on the flow direction requirements of the jet after the separation shock. This conclusion is further verified by the correlation with measured flow separation data.

Ideal Nozzle Flow Case

The classical approach for the nozzle flow adjusting to the ambient back pressure consists of an ideal one-dimensional inviscid solution with a normal shock downstream of the throat, followed by a subsonic compression to ambient pressure at the nozzle exit. This case is discussed in standard textbooks, such as Refs. 4 and 5. A more recent Note detailing the solution is found in Ref. 6. Recasting this solution as the difference of ambient pressure and the pressure upstream of the shock location vs chamber pressure gives the variation as shown in Fig. 2. Noting that, in the ideal nozzle flow solution the flow is attached to the wall at all times, the usual separation pressure is replaced by the static pressure just upstream of the normal shock.

Ideal Jet Flow Case

The other bounding case to consider is the situation of an ideal jet flow in which the flow separates off the nozzle wall to produce a balanced jet with the static pressure as ambient everywhere and with the jet flow direction as purely axial. The recovery to a balanced jet is accomplished by a special curved shock in the nozzle that simultaneously recovers ambient pressure, separates the flow from the wall, and turns the flow along the axis. Using θ_N for the local nozzle wall half-angle and using a variable upstream Mach number M_1, the criteria for the ideal jet flow case are derived as

$$p_1 = p_{\text{amb}}/\xi_{12} \tag{1}$$

with

$$\xi_{12} \equiv \frac{p_{\text{amb}}}{p_1} = \frac{2\gamma M_1^2 \sin^2\phi - (\gamma - 1)}{\gamma + 1} \tag{2}$$

$$p_c = p_1\left\{1 + [(\gamma - 1)/2]M_1^2\right\}^{(\gamma-1)/\gamma} \tag{3}$$

The shock angle is defined from an input deflection angle that is equal to the local nozzle wall half-angle. The relationship connecting the deflection angle to the shock angle involves solving a cubic equation. A closed-form solution is given in Ref. 7 with roots for a strong shock and a weak shock.

Strong shock (with corrections):

$$\sin^2\phi = \frac{k}{3} + 2\sqrt{-\frac{a}{3}}\cos\left\{\frac{1}{3}\cos^{-1}\left[\frac{-b}{2\sqrt{(-a/3)^3}}\right]\right\} \tag{4}$$

Weak shock (with corrections):

$$\sin^2\phi = \frac{k}{3} - 2\sqrt{-\frac{a}{3}}\cos\left\{\frac{\pi}{3} + \frac{1}{3}\cos^{-1}\left[\frac{-b}{2\sqrt{(-a/3)^3}}\right]\right\} \tag{5}$$

where

$$k = \frac{M_1^2 + 2}{M_1^2} + \gamma\sin^2\delta$$

$$a = \frac{2M_1^2 + 1}{M_1^4} + \sin^2\delta\left[\frac{(\gamma+1)^2}{4} + \frac{\gamma - 1}{M_1^2}\right] - \frac{k^2}{3} \tag{6}$$

$$b = \frac{k}{3}\left\{\frac{2M_1^2 + 1}{M_1^4} + \sin^2\delta\left[\frac{(\gamma+1)^2}{4} + \frac{\gamma - 1}{M_1^2}\right]\right\} - \frac{\cos^2\delta}{M_1^4} - \frac{2k^3}{27}$$

with

$$\delta = \theta_N \tag{7}$$

Through a process of incrementing the upstream Mach number M_1, the variation of separation pressure for the ideal jet flow case is shown in Fig. 3 for six representative wall angles. The shock shapes necessary to yield a balanced jet are shown in Fig. 3 for both shock types, where the strong shock is concave and normal across the axis, whereas the weak shock is convex and goes to zero strength at the axis. Because there is no mechanism to set up and maintain the shocks in the required positions, this is an ideal case only and represents the lower bound on the range of conceivable separation pressures. Flow separation data correlations will confirm that a balanced jet is not produced. Also, schlieren photographs of separated jets always show shock patterns. In an actual nozzle, the flow overexpands and requires a different set of shocks to adjust for the diverging flow and pressure drop past the ideal point. The necessary adjustment is provided by the shock structure and triple-point condition in the jet flow structure as discussed and as shown in Fig. 1.

Triple-Point Solution

Referring to the shock structure and numbering system of Fig. 1, the first feature to be noted is that the oblique shock from the separation point returns the static pressure to ambient. This is verified by nozzle pressure measurements and computational fluid dynamics calculations and is quantified as $p_4 = p_{amb}$. The second feature to be noted is that the pressure past the separation shock is uniform from the wall to the triple point, or $p_4 = p_{4tp}$. The third feature is that the Mach disk is a normal shock that appears to be curved because it follows the source flow contours of the centerline Mach number M_5. The fourth feature is that streamlines on each side of the triple point end up at an equal pressure that is above ambient, have the same flow direction, and are separated by a slipstream. The last feature forms the first triple-point boundary condition as

$$p_{6strong} = p_{6weak} = p_6 \tag{8}$$

Equation (8) is rewritten in terms of the pressure ratios across each of the shocks for the pressure boundary condition at the triple point. This states that the pressure rise across the Mach disk is equal to the combined rise through the incident and reflected shocks, i.e.,

$$\xi_{56} = \xi_{54}\xi_{46} \tag{9}$$

The second triple-point boundary condition requires equal flow angles as

$$\theta_{6weak} = \theta_{6strong} \qquad \text{or} \qquad \theta_5 + \delta_4 + \delta_{6weak} = \theta_5 + \delta_{6strong} \tag{10}$$

With a normal shock at the Mach disk, $\delta_{6strong} = 0$; thus,

$$\delta_4 + \delta_{6weak} = 0 \tag{11}$$

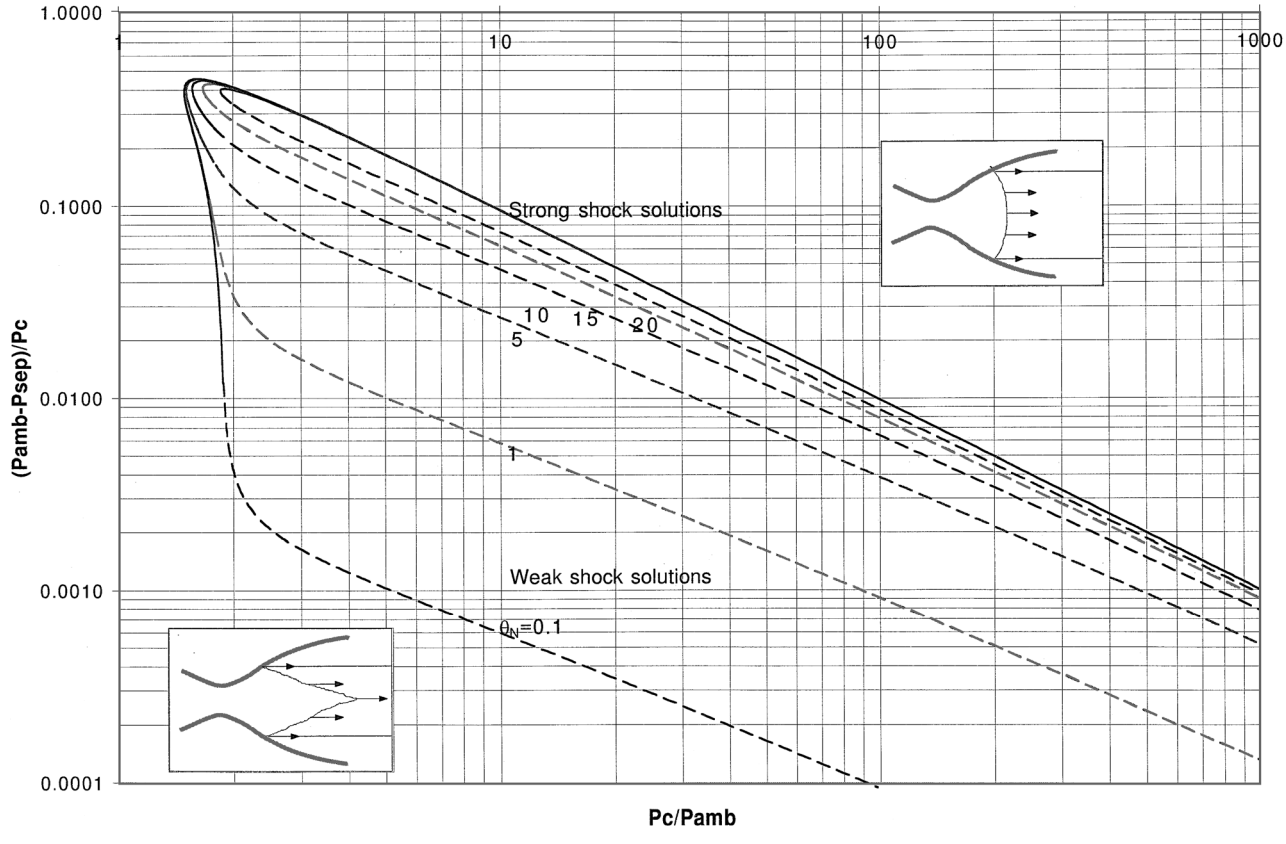

Fig. 3 Separation pressure from ideal jet flow case.

Noting that the deflection through the incident shock is negative, Eq. (11) is then written in terms of the shock strengths and upstream Mach numbers through the standard oblique shock and isentropic flow relationships to become

$$\left(\frac{\xi_{54}-1}{\gamma M_5^2-\xi_{54}+1}\right)^2 \frac{2\gamma M_5^2-(\gamma+1)\xi_{54}-(\gamma-1)}{(\gamma+1)\xi_{54}+(\gamma-1)}$$

$$= \left(\frac{\xi_{46}-1}{\gamma M_{4\text{tp}}^2-\xi_{46}+1}\right)^2 \frac{2\gamma M_{4\text{tp}}^2-(\gamma+1)\xi_{46}-(\gamma-1)}{(\gamma+1)\xi_{46}+(\gamma-1)}$$

where

$$M_{4\text{tp}}^2 = \frac{M_5^2[(\gamma+1)\xi_{54}+(\gamma-1)]-2\left(\xi_{54}^2-1\right)}{\xi_{54}[(\gamma-1)\xi_{54}+(\gamma+1)]}$$

$$p_5 = p_c\left[1+\frac{(\gamma-1)}{2}M_5^2\right]^{[-\gamma/(\gamma+1)]}$$

$$p_6 = p_5\left[\frac{2\gamma M_5^2-(\gamma-1)}{(\gamma+1)}\right] \tag{12}$$

$$\xi_{54}=\frac{p_{\text{amb}}}{p_5}, \qquad \xi_{56}=\frac{p_6}{p_5}, \qquad \xi_{46}=\frac{p_6}{p_{\text{amb}}}$$

The solution of Eqs. (9) and (12) can best be illustrated by a shock polar or pressure deflection diagram. Figure 4 presents the shock polar for a centerline Mach number of $M_5 = 3.2278$, which, to satisfy the triple-point conditions, must be shocked by the incident wave to $M_{4\text{tp}} = 2.1289$. The reflected wave further shocks the flow to $M_{6\text{weak}} = 1.3320$. The intercept of the Mach disk and the reflected wave is shown by the open circle, where both the pressure requirement of Eq. (9) and the flow angle requirement of Eq. (11) are satisfied.

The shock polar of Fig. 4 is constructed for a known centerline Mach number with a variable chamber pressure, thus, centerline pressure. The relationship of a given centerline Mach number to the chamber pressure and the separation Mach number is found by the following observation and its consequences. It is noted that the shock cells in a separated jet repeat until viscous effects smear them out. The repetitive nature implies that the jet pressure continues to oscillate about the ambient value as it goes from overexpanded to underexpanded. The postulation made in this analysis is that the overexpansion equals the underexpansion. The degree of over/underexpansion is measured by the pressure ratio across the separation shock and the reflected shock; thus, the requirement

$$p_{\text{amb}}/p_{\text{sep}} = p_6/p_{\text{amb}} \tag{13}$$

or in symbol notation,

$$\xi_{34} = \xi_{46}$$

Expanding, Eq. (13) becomes

$$\xi_{34}^2 = \xi_{56}(p_5/p_3)$$

and solving for chamber pressure as a function of wall and centerline Mach numbers gives

$$\frac{p_c}{p_{\text{amb}}} = \left\{\left[1+\frac{(\gamma-1)}{2}M_3^2\right]^{\gamma/(\gamma-1)} \Big/ \left[\frac{2\gamma M_5^2-(\gamma-1)}{(\gamma+1)}\right]^{\frac{1}{2}}\right\}$$

$$\times \left\{\left[1+\frac{(\gamma-1)}{2}M_5^2\right]\Big/\left[1+\frac{(\gamma-1)}{2}M_3^2\right]\right\}^{\gamma/2(\gamma-1)} \tag{14}$$

The simultaneous solution of Eqs. (9), (12), and (14) yields a singularly unique solution for the separation Mach number, the centerline Mach number, and the chamber pressure. This relationship is shown in Fig. 5 for air. No solution was found below $M_3 = 2.254$ due to the separation shock strength going to one, $M_5 \to M_3$, and $A_{\text{Md}} \to A_3$.

The combined shock polar from the wall through the triple point is shown in Fig. 6 for a wall Mach number $M_3 = 3$. The conditions

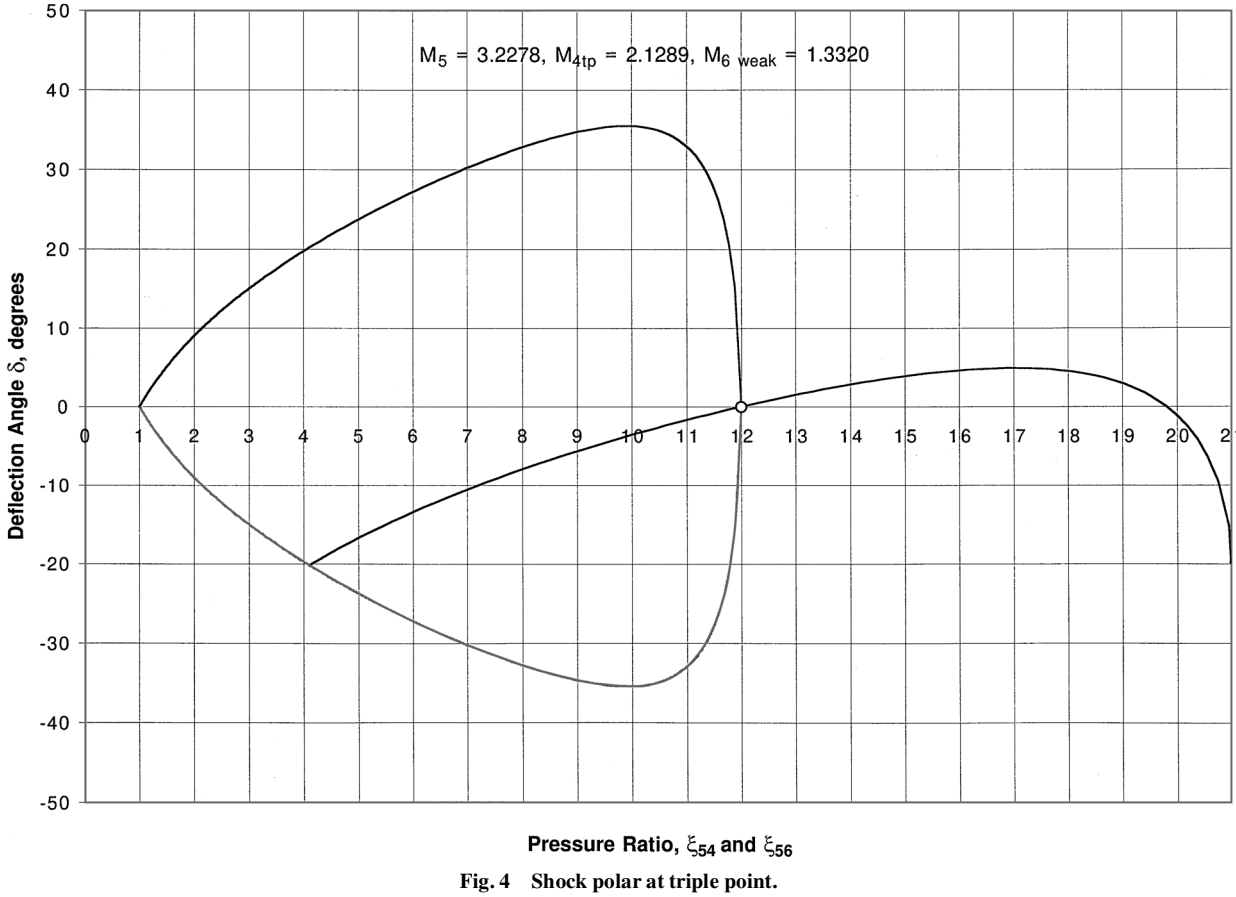

Fig. 4 Shock polar at triple point.

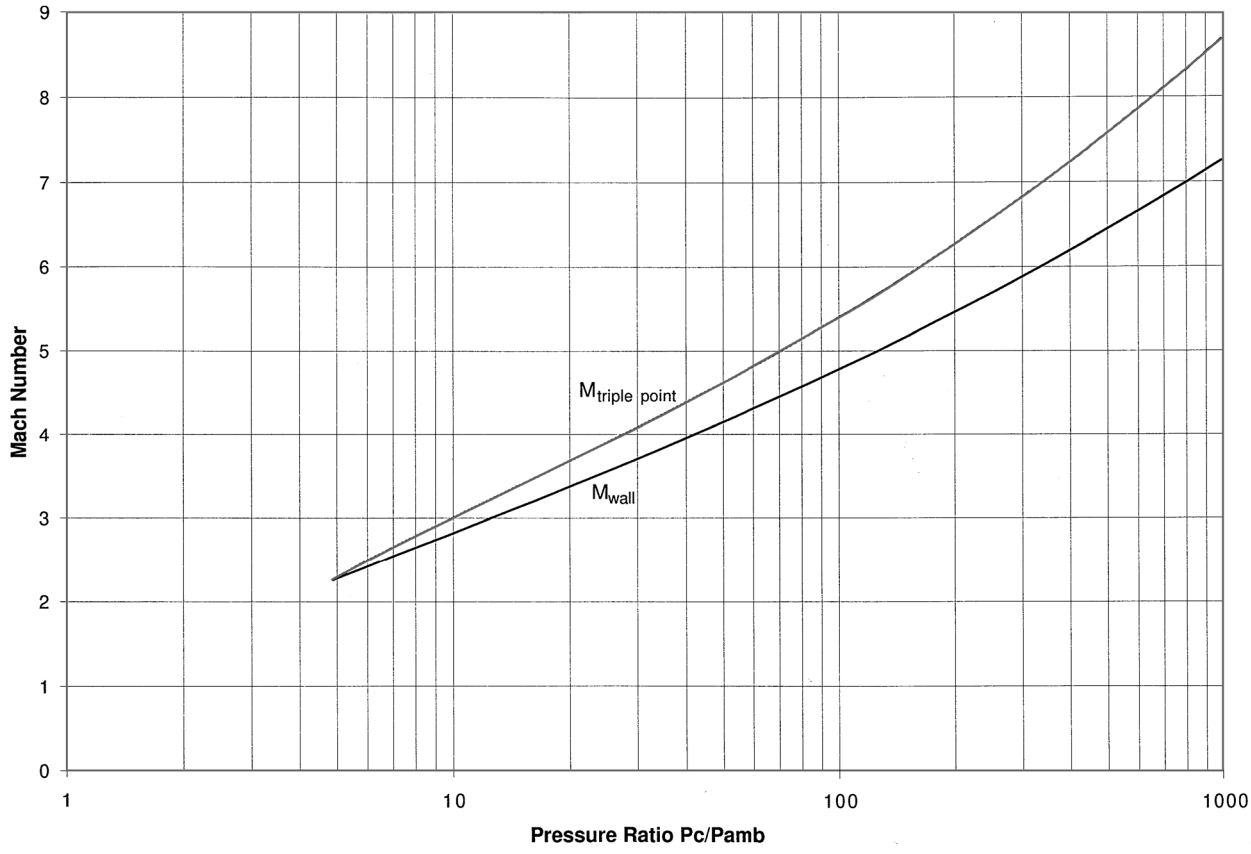

Fig. 5 Mach numbers at wall and triple point.

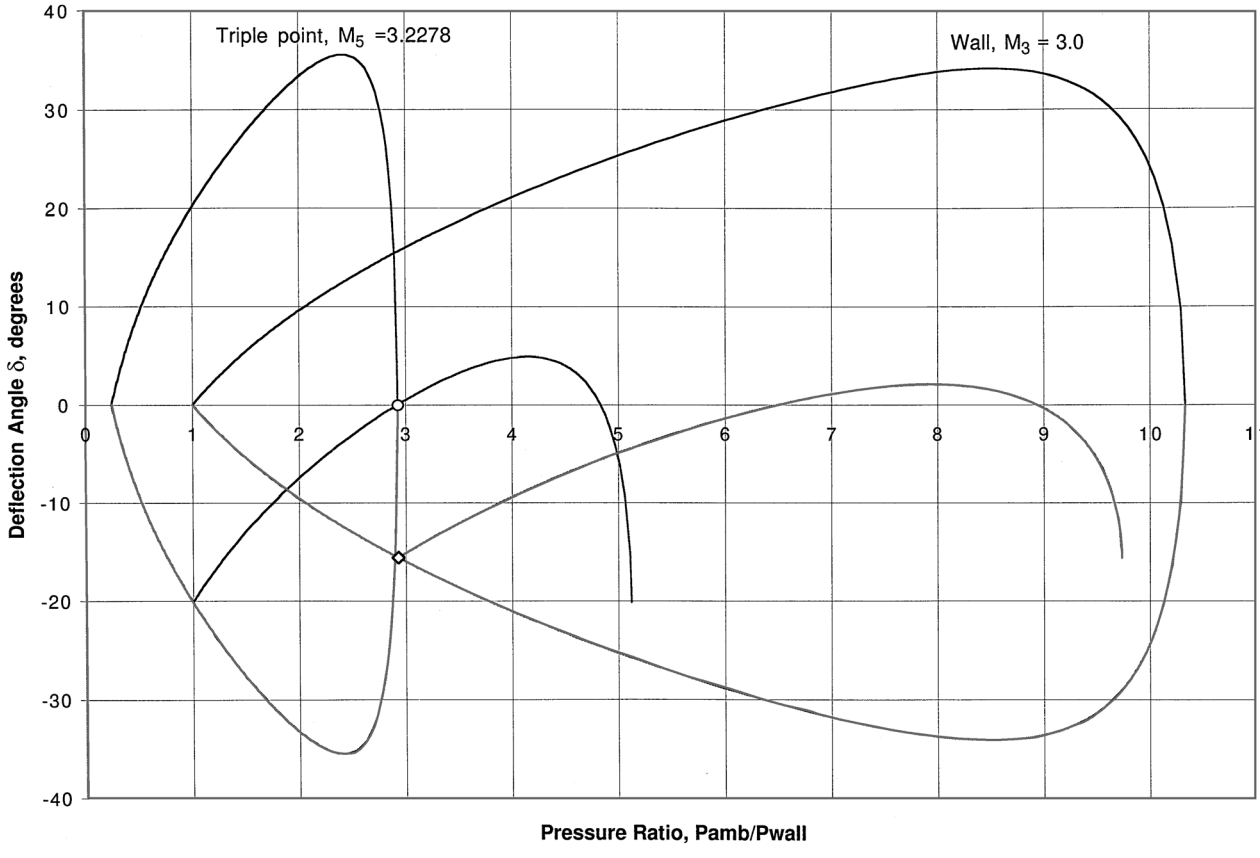

Fig. 6 Combined shock polar for wall and triple point.

of Eqs. (9), (12), and (14) are denoted by the open circle from the centerline shock polar and the open diamond for the wall shock polar and Eq. (14).

The separation pressure is then obtained from isentropic relations as

$$\frac{p_{\text{amb}}}{p_{\text{sep}}} = \frac{p_{\text{amb}}}{p_c}\left[1 + \frac{(\gamma-1)}{2}M_3^2\right]^{\gamma/(\gamma-1)} \tag{15}$$

Normal Shock Solution

No triple-point solution is found below $M_3 = 2.254$ because the Mach disk has reached the wall. Another jet flow situation is suggested by this result, where a normal shock starts at the wall and curves across the axis. The jet produced is above ambient pressure downstream of the normal shock and is also unbalanced by flow direction, requiring expansion waves to adjust the flow similar to the second half of the shock cell of the triple-point solution. In actual nozzle flow situations, the normal shock will interact with the boundary layer and still produce a lambda shock feature. This is the feature that forced a focus on the boundary layer as the causal factor to flow separation starting with the original schlieren photographs by Prandtl in 1907 (Ref. 4, p. 276).

The normal shock solution may also be expressed by the over/underexpansion criterion of Eq. (13) and by Eq. (14) with M_5 replaced by M_3:

$$\frac{p_c}{p_{\text{amb}}} = \left[1 + \frac{(\gamma-1)}{2}M_3^2\right]^{\gamma/(\gamma-1)} \Bigg/ \left[\frac{2\gamma M_3^2 - (\gamma-1)}{(\gamma+1)}\right]^{\frac{1}{2}} \tag{16}$$

The separation pressure from the triple-point solution is shown in Fig. 7 along with the normal shock solution for comparison. It is anticipated that the triple-point solution is valid down to a separation Mach number of $M_3 = 2.254$ and the normal shock solution for lower Mach numbers. Data correlations will be discussed to show the applicability of the two solutions.

Balance of Mass and Momentum

A complete picture of the shock cell requires a specification of the size of the Mach disk. This is provided by a mass and momentum balance between the separation point and upstream of the Mach disk at point 5, as shown in Fig. 1. The mass flux at point 5 is specified above (tp+) and below the triple point (tp−) as

$$\dot{m}_3 = \dot{m}_5 = \dot{m}_{\text{tp}+} + \dot{m}_{\text{tp}-}$$

or

$$\rho_3 A_3 V_3 = \bar{\rho}_4 A_4 \bar{V}_4 + \rho_5 A_{\text{Md}} V_5$$

with

$$\bar{V}_4 = \frac{V_4 + V_{4\text{tp}}}{2}$$

thus,

$$\bar{\rho}_4 A_4 = \frac{\rho_3 A_3 V_3 - \rho_5 A_{\text{Md}} V_5}{\bar{V}_4}$$

Also

$$\rho_3 A_3 V_3 = \bar{\rho}_5 A_5 \bar{V}_5 = (\bar{\rho}_4 A_4 + \rho_5 A_{\text{Md}})\bar{V}_5$$

giving

$$\frac{\bar{V}_5}{V_3} = 1 \Bigg/ \left[\frac{V_3}{\bar{V}_4} + \alpha\frac{\rho_5}{\rho_3}\left(1 - \frac{V_5}{\bar{V}_4}\right)\right] \tag{17}$$

where $\alpha = A_{\text{Md}}/A_3$. The thrust balance is

$$F_3 = F_5$$

$$\dot{m}_3 V_3 + (p_3 - p_{\text{amb}})A_3 = \dot{m}_3 \bar{V}_5 + (p_5 - p_{\text{amb}})A_{\text{Md}}$$

$$\gamma C_D M_3^2 + (1 - \xi_{34}) = \gamma C_D M_3^2(\bar{V}_5/V_3) + (\xi_{35} - \xi_{34})\alpha$$

Finally,

$$\frac{\bar{V}_5}{V_3} = 1 - \frac{\xi_{34} - 1 + (\xi_{35} - \xi_{34})\alpha}{\gamma C_D M_3^2} \tag{18}$$

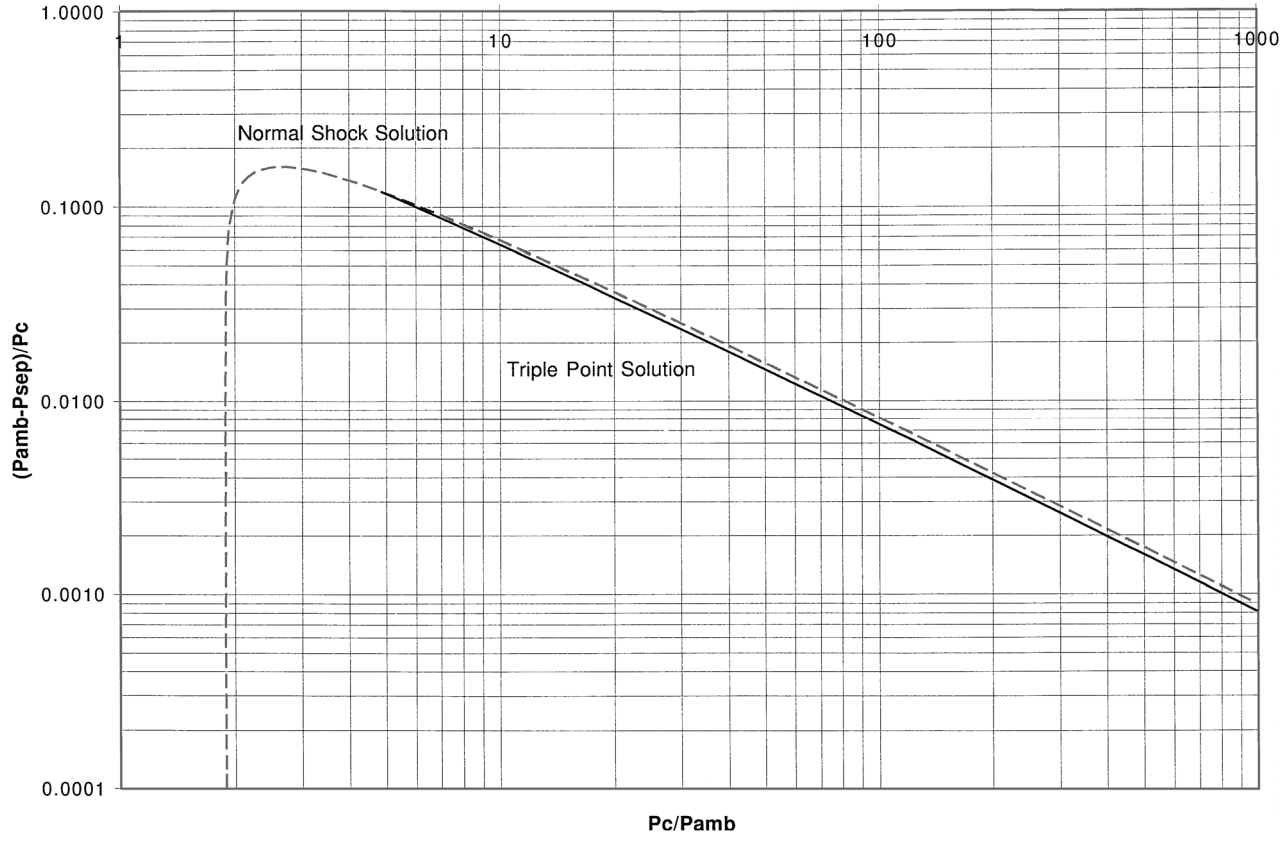

Fig. 7 Derived solutions for nozzle flow separation.

From the mass flux equation (17) and the thrust equation (18) the Mach disk area becomes a quadratic function as

$$\gamma C_D M_3^2 = \{(V_3/\bar{V}_4) + \alpha(\rho_5/\rho_3)[1 - (V_5/\bar{V}_4)]\}$$
$$\times \left[\left(\gamma C_D M_3^2 - \xi_{34} + 1\right) - (\xi_{35} - \xi_{34})\alpha\right]$$

Thus,

$$\alpha = \frac{-b + \sqrt{b^2 - 4ac}}{2a} \tag{19}$$

with

$$a = (\rho_5/\rho_3)[1 - (V_5/\bar{V}_4)](\xi_{35} - \xi_{34})$$

$$b = (V_3/\bar{V}_4)(\xi_{35} - \xi_{34}) - (\rho_5/\rho_3)[1 - (V_5/\bar{V}_4)]\left(\gamma C_D M_3^2 - \xi_{34} + 1\right)$$

and

$$c = \gamma C_D M_3^2[1 - (V_3/\bar{V}_4)] + (V_3/\bar{V}_4)(\xi_{34} - 1)$$

Results give a ratio of Mach disk to separation point radius of 1.0 for $M_3 = 2.254$, which decreases to 0.85 for $M_3 = 7.25$. This is in contrast to a recently published paper[8] on two-dimensional jets with Mach disk heights that range from 0 to 0.7 for a given M_3. Applying Eq. (13) to an overexpanded nozzle yields only one jet solution without assumptions about the Mach disk shape or slipstream shape. As pointed out in Ref. 9, axisymmetrical effects occur very near the axis and force the shock to be normal, which is already in the present solution and is, therefore, comparable to the two-dimensional solution addressed in Ref. 8.

Further, confirmation of the applicability of Eq. (13) to a freejet from an overexpanded nozzle is offered from the classical literature. Prandtl (Ref. 4, p. 266) published a schlieren photograph from L. Mach, taken in 1897, which shows six visible shock cells from an overexpanded nozzle. All six shock cells are of equal length, which to this author implies that the jet is equally overexpanded and underexpanded as Eq. (13) states.

Data Correlation

Schilling[3] collected a total of 409 data points from the industry as of 1962. These were grouped in sets for six conical nozzles, short contoured nozzles with exit half-angles from 7 to 13.5 deg, and long contoured nozzles with exit half-angles from 4 to 6 deg. The data were initially shown in the usual form of p_{sep}/p_{amb} vs p_c/p_{amb}; however, the data scatter was very large, forcing Schilling to look for other correlation parameters. One was found from Green,[10] where the term $(p_{amb} - p_{sep})/p_c$ vs p_c/p_{amb} was suggested based on that form being in the thrust equation. Schilling found there to be a dramatic collapse of all of the data by using Green's parameter.

Figure 8 compares the new solution for flow separation to the short contoured nozzle data in terms of Green's parameter. The correlation is extremely good, providing confirmation of the present model with the assumptions that the separation is driven by the pressure adjustment process in the separated jet and that the degree of underexpansion is equal to the degree of overexpansion. A total of 91 data points was collected by Schilling for short contoured nozzles from Ref. 3 (with unpublished Pratt and Whitney data) and Refs. 11 and 12. These data points are shown in Fig. 8 and are the most applicable to the SRMU nozzle. The data trends of the conical nozzles and the long contoured nozzles are similar. The magnitudes of Green's parameter from the 5-, 10-, and 15-deg conical nozzles and the long contoured nozzles vary by only ±3.5% from the short contoured nozzles. This illustrates the minimal effects that nozzle half-angle and boundary-layer characteristics have on the flow separation phenomena. Contoured nozzles will have a similarly small effect as the nozzle lip curves toward the separated jet and restricts entrainment inflow inside the nozzle, thus altering the local ambient pressure downstream of the separation point.

Another point to be made about the correlation of data to the two solutions of this report is that the data match only the triple-point solution and do not line up with the normal shock solution. It was anticipated that perhaps there would be a match below the range of the triple-point solution, or below $M_3 = 2.254$ and a chamber-pressure-to-ambient ratio p_c/p_{amb} of 4.8. However, there are no data in the Schilling report below a p_c/p_{amb} of 5.2 to determine its applicability.

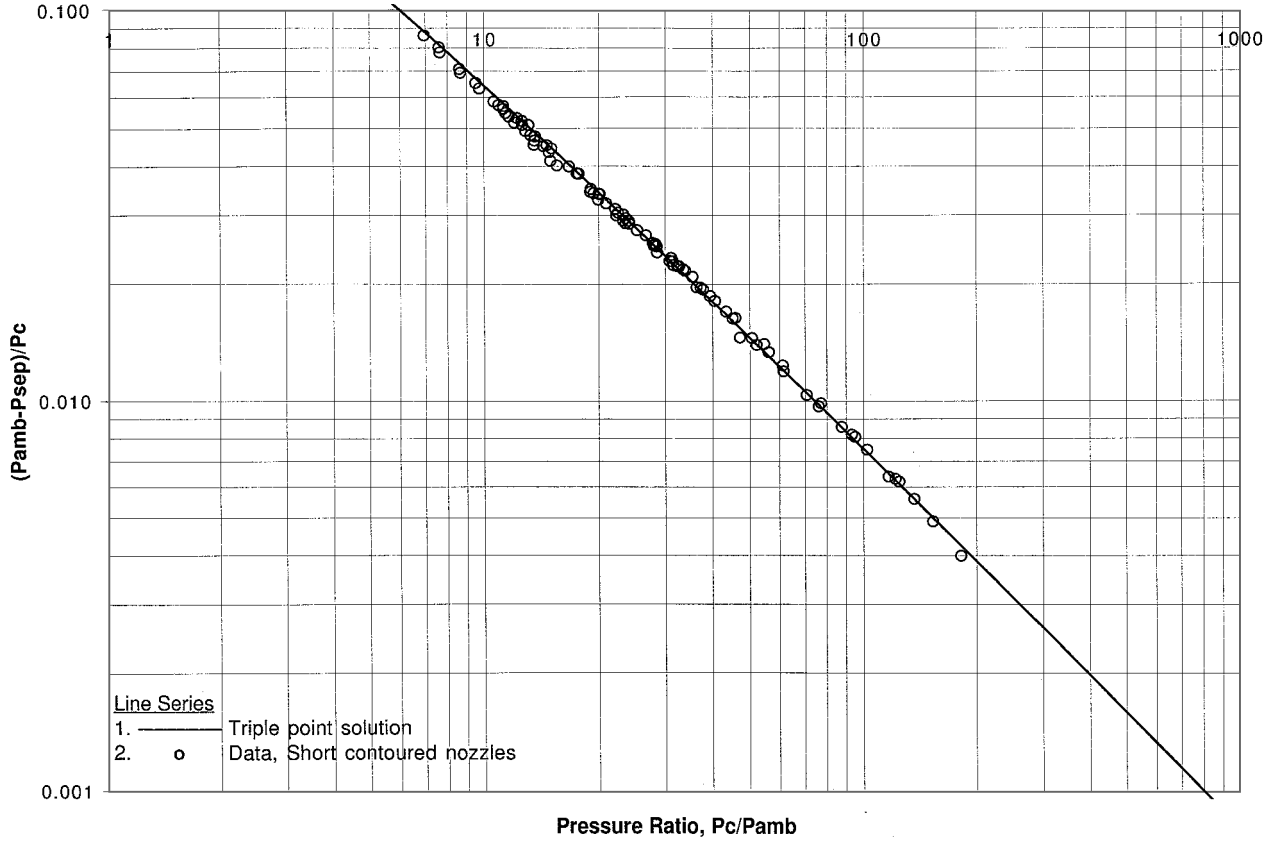

Fig. 8 Comparison of triple-point solution with separation data.

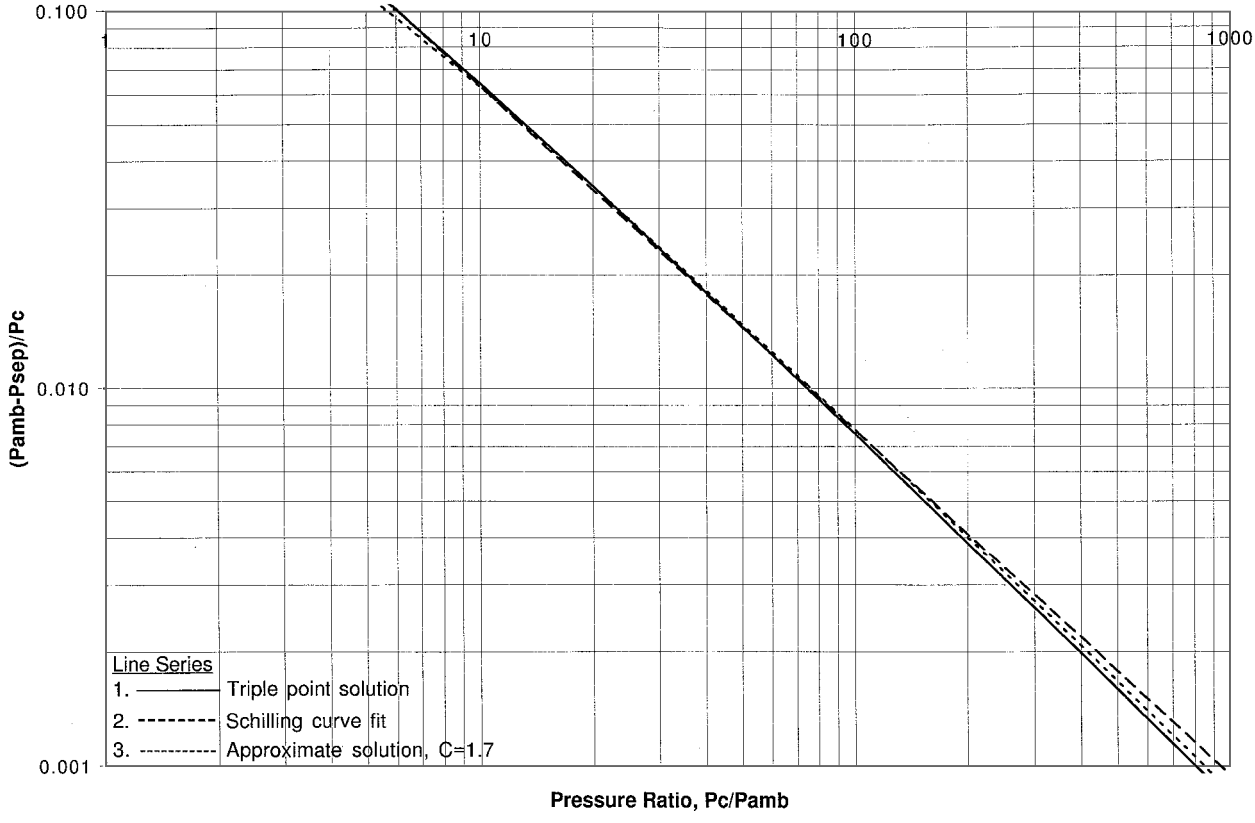

Fig. 9 Camparison of solutions for flow separation.

Approximate Solution

The thrust balance in Eq. (18) can be rewritten for the separation Mach number as

$$M_3^2 = \frac{\xi_{34} - 1 + (\xi_{35} - \xi_{34})\alpha}{\gamma C_D[1 - (\bar{V}_5/V_3)]}$$

This equation is closely approximated with

$$M_3^2 \cong \frac{B\left(\xi_{34}^2 - 1\right)}{\gamma C_D} \tag{20}$$

where $B = 1.7$.

Schilling Curve Fit

The work of Schilling is also important in that he found that, if the data points are plotted in terms of Green's parameter, they are closely matched by a straight line on a log–log plot. The simple form of the empirical separation criteria found by Schilling is

$$\frac{p_{\text{amb}} - p_{\text{sep}}}{p_c} = C\left(\frac{p_c}{p_{\text{amb}}}\right)^E \tag{21}$$

where C and E are constants for each of the nozzle groups. For short contoured nozzles, $C = 0.517$ and $E = -0.913$. This form is easily adapted to a spreadsheet calculation and can readily handle new data through variation of the constant C and exponent E.

A comparison of the triple-point solution, the approximate solution, and the Schilling curve fit for short contoured nozzles is made in Fig. 9. Because the approximate form and the empirical form correlate so well with the direct solution and with the data of Fig. 8, it should be considered that this provides a validation for their use, and either one should be more than adequate for engineering-trade studies.

Summary and Conclusions

For any given chamber pressure and ambient pressure, it is shown that flow separation in the nozzle is a direct result of the flow adjusting to a constant back pressure. A focus on the overall jet shock structure, which is responsible for the separation shock, has yielded a direct calculation of the flow separation pressure and location. This is accomplished by a pressure and flow direction balance at the jet triple point and by the assumption of a pressure condition in the jet repeating shock cells, which oscillates equally from overexpanded to underexpanded. Also, an approximate solution is found that differs very little from the triple-point solution. Furthermore, the use of either the approximate model or the Schilling curve fit is justified when performing engineering estimates of flow separation and flow separation side loads.

References

[1] Morrisette, E. L., and Goldberg, T. J., "Turbulent-Flow Separation Criteria for Overexpanded Supersonic Nozzles," NASA TP-1207, Aug. 1978.

[2] Arens, M., and Spiegler, E., "Shock-Induced Boundary Layer Separation in Overexpanded Conical Exhaust Nozzles," *AIAA Journal*, Vol. 1, No. 3, 1963, pp. 578–581.

[3] Schilling, M., "Flow Separation in a Rocket Nozzle," M.S. Thesis, Graduate School of Arts and Sciences, Univ. of Buffalo, Buffalo, NY, June 1962.

[4] Prandtl, L., *Essentials of Fluid Dynamics*, Blackie, Glasgow, Scotland, UK, pp. 266, 269, 276 (translation).

[5] Shapiro, A. H., *The Dynamics and Thermodynamics of Compressible Fluid Flow*, Ronald Press, New York, 1953, p. 93.

[6] Liou, M.-S., "Solutions of One-Dimensional Steady Nozzle Flow Revisited," *AIAA Journal*, Vol. 26, No. 5, 1988, pp. 625–628.

[7] Briggs, J. L., "Comment on Calculation of Oblique Shock Waves," *AIAA Journal*, Vol. 2, No. 5, 1964, p. 974.

[8] Li, H., and Ben-Dor, G., "Mach Reflection Wave Configuration in Two-Dimensional Supersonic Jets of Overexpanded Nozzles," *AIAA Journal*, Vol. 36, No. 3, 1998, pp. 488–491.

[9] Ferri, A., "Supersonic Flow with Shock Waves," *General Theory of High Speed Aerodynamics, High Speed Aerodynamics and Jet Propulsion*, edited by W. R. Sears, Vol. 6, Princeton Univ. Press, Princeton, NJ, 1954, p. 677.

[10] Green, L., "Flow Separation in Rocket Nozzles," *ARS Journal*, Vol. 23, No. 1, 1953, pp. 34, 35.

[11] Farley, J. M., and Campbell, C. E., "Performance of Several Method-of-Characteristic Exhaust Nozzles," NASA TN-D-293, Oct. 1960.

[12] Ahlberg, J. H., Hamilton, S., Migdal, D., and Nilson, E. N., "Truncated Perfect Nozzles in Optimum Nozzle Design," *ARS Journal*, Vol. 31, No. 5, 1961, pp. 614–620.

P. R. Bandyopadhyay
Associate Editor